Chinese Chemical Letters 35 (2024) 109213

Contents lists available at ScienceDirect

Chinese Chemical Letters

journal homepage: www.elsevier.com/locate/cclet

Boosting the electrochromic properties by large V_2O_5 nanobelts interlayer spacing tuned *via* PEDOT

Haohao Sun[a], Wenxuan Wang[a], Yuli Xiong[a,b,*], Zelang Jian[a,*], Wen Chen[a]

[a] State Key Laboratory of Advanced Technology for Materials Synthesis and Processing, School of Materials Science and Engineering, Wuhan University of Technology, Wuhan 430070, China
[b] Sanya Science and Education Innovation Park of Wuhan University of Technology, Sanya 572000, China

ARTICLE INFO

Article history:
Received 18 April 2023
Revised 29 July 2023
Accepted 16 October 2023
Available online 21 October 2023

Keywords:
Vanadium oxide
PEDOT
Nanobelts
Interlayer spacing
Electrochromic

ABSTRACT

Vanadium pentoxide (V_2O_5) with a layered structure is of great interest in the field of electrochromic (EC) due to its abundance of color variations. However, there are still a series of problems such as slow ion diffusion, poor electronic conductivity and cyclic stability in the reaction process. Herein, we successfully prepared a stable and fast multi-color electrochromic material V_2O_5-PEDOT by a simple "one-pot" method. The layer space of V_2O_5 could be tuned by 3,4-ethylenedioxythiophene (named V_2O_5-PEDOT) during the dissolution and recrystallization of vanadium oxide. The expanded layer spacing facilitates rapid ion insertion and extraction. PEDOT serves as an internal conductive pillar to improve the overall conductivity of the material. The obtained intercrossing structure of the nanobelts shortens the ion diffusion distance and ensures electrolyte penetration. The V_2O_5-PEDOT exhibits the fast response time (1.1 s for coloration and 3.5 s for bleaching at 422 nm), high optical contrast ($\Delta T = 45\%$ at 422 nm and $\Delta T = 35.2\%$ at 1000 nm), great coloration efficiency (CE = 97.1 cm^2/C), and high cyclic stability (86% preserved after 3000 cycles). The electrochromic devices (ECD) were successfully assembled by using V_2O_5-PEDOT films as ion storage layers and electrochromic layers, demonstrating remarkable performance.

Electrochromic is the ability in which a material or device changes its optical properties in response to the applied voltage [1–3]. Due to the transmission or reflection properties and ability to function in the visible or infrared spectral range, electrochromic devices (ECD) can be used in a variety of situations, including smart windows, rearview mirrors, and protective eyewear [4–6]. In comparison to other electrochromic materials, V_2O_5 as a layered metal oxide has the advantages of a high guest ion density, good interaction with molecules or ions, natural abundance, and low cost. Significantly, it has distinct optical and electrochemical characteristics [7,8]. However, insufficient layer spacing, poor electrical conductivity and poor cycling stability limit its electrochemical performance [9–12]. To overcome these issues, one of the successful strategies is to synthesize V_2O_5 with nanostructures.

V_2O_5 with nanostructures, such as nanobelts, nanowires, and nanorods, could provide abundant surficial active sites, and exhibit short ion insertion/extraction distances [9,13-15]. In addition, conductive polymers can be added to form nanocomposites, which can enhance electrochromic properties. These nanocomposites have a synergistic effect [16], which inherit the advantages of the V_2O_5 itself, as well as the good charge transport properties offered by the conductive polymers. This combination of properties can make these nanocomposites useful in a variety of applications, such as energy storage devices, sensors, and electrochromic devices. Zhang *et al.* obtained polyaniline-coated V_2O_5 nanowires by chemical oxidative polymerization, which were able to reduce volume expansion during cycling and increase the stability (1000 cycles) and polychromatic of the material [17]. Li *et al.* synthesized superlattice nanocomposite by using aniline's oxidative polymerization between layers of V_2O_5 [18]. Unfortunately, the potential presence of benzidine groups in the polymer backbone, which might degrade into hazardous (carcinogenic) compounds, limits the applicability of these nanocomposites [19]. PEDOT as an environmentally friendly conductive polymer has greater stability and conductivity than that of polypyrrole or polyaniline [20]. Its applications in supercapacitors and ion batteries have been studied extensively [21,22]. However, in the field of electrochromic, due to the insolubility of PEDOT itself. It is still used for electrochromic applications together with poly(3,4-ethylenedioxythiophene)-doped poly(styrene sulfonic acid) (PEDOT:PSS). Ling *et al.* preparation of multilayer hybrid films of PEDOT:PSS and WO_3 NPs using a layer-

* Corresponding authors.
E-mail addresses: yuli.xiong@whut.edu.cn (Y. Xiong), zelangjian@whut.edu.cn (Z. Jian).

https://doi.org/10.1016/j.cclet.2023.109213
1001-8417/

by-layer assembly method [23]. In these materials, PSS acts as an insulator without any electrochromic properties. It might inhibit charge transfer between PEDOT and WO_3, even the electrochromic redox process [24]. Therefore, to overcome these issues, we directly utilized the strong oxidation properties of V_2O_5 to obtain V_2O_5-PEDOT nanobelts by an intercalation polymerization with EDOT.

In addition, it was found that the use of *in situ* intercalation polymerization of conducting polymers allows for the expansion of the layer spacing and facilitates the improvement of electrochemical properties. Kuchena *et al.* reported the synthesis of PANI intercalated V_2O_5 nanoflowers with a layer spacing of 13.99 Å between V-O layers by intercalation polymerization, resulting in larger diffusion channels, enhanced specific surface area and improved ammonia ion (de)intercalation kinetics [25]. Bin *et al.* reported the preparation of a PEDOT-$NH_4V_3O_8$ (PEDOT-NVO) aqueous zinc battery, and the results showed that the expanded interlayer spacing (10.8 Å) achieved through polymer intercalation was the primary reason for the improved electrochemical performance [26]. Electrochromic has a similar structure and operating principle to batteries and supercapacitors [27]. Therefore, we believe that expanding the V_2O_5 layer spacing is a useful strategy to improve the electrochromic performance.

Herein, we present a simple in situ intercalation polymerization method to obtain V_2O_5-PEDOT nanobelts. The V_2O_5 nanobelts are used as a core to maintain both the polychromatic nature of V_2O_5 itself and the shortened ion/electron transport distances. Organic molecules can be inserted between the layers to act as anchors and reduce volume expansion. Especially when they are polymerized in a sandwich, these internal conductive polymers are highly conductive, they can also be used as internal electronic conductors. In addition, we can take advantage of the enlarged layer spacing of V_2O_5 (13.4–17.5 Å) with the insertion of PEDOT to solve the problem of the narrow layer spacing of V_2O_5 (4.38 Å) and increase the migration rate of ions, thus improving the electrochromic performance. The results show that V_2O_5-PEDOT nanobelts have excellent electrochromic performance. Notably, when EDOT is 1 mL (V_2O_5–1.0PEDOT), it exhibits the fast response time (1.1 s for coloration and 3.5 s for bleaching at 409 nm), high optical contrast ($\Delta T = 45\%$ at 422 nm and $\Delta T = 35.2\%$ at 1000 nm) and high cyclic stability (86% preserved after 3000 cycles). Subsequently, the ECD's performance was evaluated.

The formation of V_2O_5-PEDOT nanobelts can be illustrated in Scheme 1. Commercial V_2O_5 shows an irregular bulk morphology with an average diameter of about 1–2 μm (Figs. S1a and b in Supporting information). After mixing with EDOT and stirring at room temperature for several hours, V_2O_5-PEDOT nanobelts formed with the size of lengths of several micrometers and widths of about 10–50 nm (Fig. S2 in Supporting information) and the color of the mixture changed from orange to dark green (Fig. S2 inset), which is attributed to the different degree of reduction of V^{5+} caused by EDOT [28]. The formation of V_2O_5-PEDOT can be described by anti-Ostwald maturation mechanism as follows [29,30]: Commercial V_2O_5 is slightly soluble in water and produce vanadium oxide species. With the increase of the stirring time, the concentration of vanadium species increases until that the V_2O_5 is totally dissolved and re-assembled to form nanobelts. And in the process, due to the high valence state of V^{5+}, V_2O_5 itself can act as an oxidant, so that under prolonged stirring, EDOT can slowly polymerize under the oxidation of V_2O_5 to form PEDOT layers inserted between the V_2O_5 layers [31]. In addition, the prepared V_2O_5 nanobelts without adding EDOT are shown in Figs. S1c and d (Supporting information). The interlayer spacing can be expanded by polymerizing EDOT in the V_2O_5 layer, and the interlayer spacing is adjustable from 13.4 Å to 17.5 Å by varying the EDOT content [32]. The unique PEDOT intercalated ultrathin nanobelt structures are expected to shorten the ion diffusion distance and accelerate the Li^+ diffusion kinetic for designing high-performance electrochromic materials.

As shown in Figs. 1a-c insets, the interlayers spacing of V_2O_5–0.5PEDOT and V_2O_5–1.0PEDOT are 1.34 nm and 1.40 nm, respectively, which is consistent with the interlayer spacing of monolayer PEDOT intercalated V_2O_5 [16]. The interlayer spacing of V_2O_5–1.5PEDOT is about 1.75 nm, which is close to the distance of the bilayer PEDOT insertions to the V_2O_5 layer in the literature [14]. EDS mappings confirm the uniform distribution of V, O and C in the nanobelts for all samples (Fig. 1d and Fig. S3 in Supporting information). Fig. S4 (Supporting information) shows the XRD pattern of commercial V_2O_5 powders with an orthorhombic structure (JCPDS No. 41–1426). The diffraction peak at 20.31° is indexed to the (001) plane, which corresponds to an interlayer spacing of 4.38 Å. However, all V_2O_5-PEDOT samples present the monoclinic structure [33], and the peaks of (001) plane shifts to lower angles (Fig. 1e). The low-angle diffraction peaks of V_2O_5–0.5PEDOT, V_2O_5–1.0PEDOT, and V_2O_5–1.5PEDOT are 6.61°, 6.34°, and 5.03°, respectively, corresponding to *D*-spacing of 1.335, 1.392, and 1.754 nm, respectively, which are close to the spacing of the layers measured by TEM (Fig. S4b). Additionally, the three samples show new diffraction peaks at ~9.38° corresponding to the (002) crystal plane. Furthermore, with the increase of PEDOT content, the intensity of (001) peak drastically decreased, which may be caused by the destruction of lattice periodicity [34] and the presence of amorphous phases of PEDOT [35]. From the TG and DSC curves (Fig. S5 in Supporting information), there is a slight weight loss

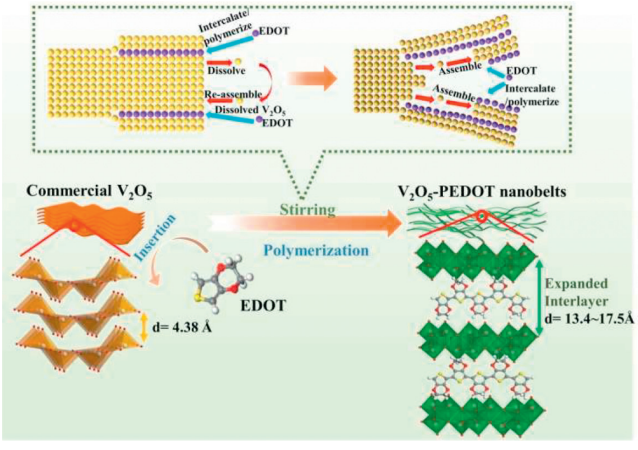

Scheme 1. Schematic illustration of V_2O_5-PEDOT nanobelts' preparation.

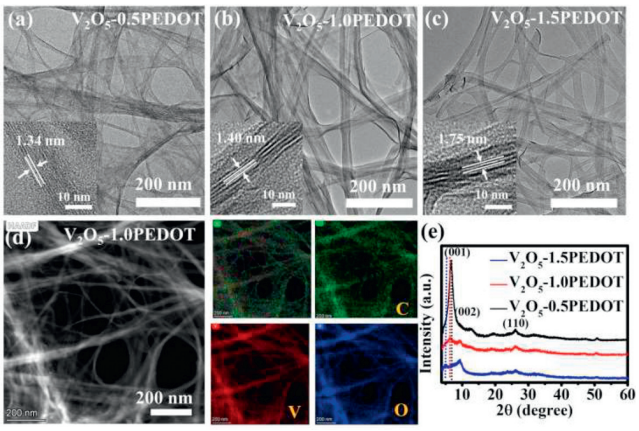

Fig. 1. TEM images and HRTEM images of (a) V_2O_5–0.5PEDOT, (b) V_2O_5–1.0PEDOT and (c) V_2O_5–1.5PEDOT. (d) EDS elemental maps of V_2O_5–1.0PEDOT. (e) XRD patterns.

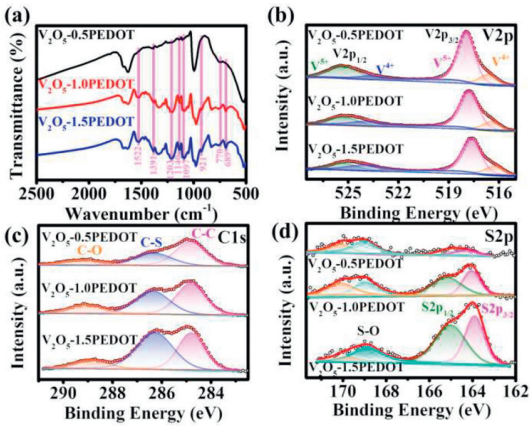

Fig. 2. (a) FTIR spectra. XPS spectra of (b) V 2p, (c) C 1s, (d) S 2p obtain from V_2O_5–0.5PEDOT, V_2O_5–1.0PEDOT and V_2O_5–1.5PEDOT.

at ~120 °C due to the physically adsorbed water [19]. The weight loss at ~206 °C is the contribution of interlayer water, and the weight loss at 368 °C is attributed to the decomposition of PEDOT, which agrees with the exothermic peak in the DSC curve. The heat absorption peak at 650 °C is due to the crystallization of V_2O_5 [25]. The PEDOT contents for V_2O_5–0.5PEDOT, V_2O_5–1.0PEDOT, and V_2O_5–1.5PEDOT samples are calculated to be 3.5%, 9.7%, and 16.2%, respectively. TG and DSC tests were performed to further demonstrate the existence and amount of PEDOT in the V_2O_5-PEDOT samples.

Fig. S6 (Supporting information) shows the FTIR spectrum of commercial V_2O_5. Peaks at 596 and 828 cm^{-1} belong to the V-O-V symmetric and asymmetric stretching modes, respectively, and the peak at 1017 cm^{-1} is associated with the V=O stretching vibration. While the position and shape of the vibration peak of V_2O_5-PEDOT samples changed significantly (Fig. 2a), in which the V-O-V stretching mode and asymmetric stretching mode were shifted to 521 cm^{-1} and 827 cm^{-1}, and the V=O stretching mode was shifted to 978 cm^{-1}. This may be caused by the greater number of V^{4+} centers present in the nanocomposite [19]. The peaks at 1522 and 1391 cm^{-1} are caused by the aromatic C=C and C-C stretching in the thiophene ring. The peaks at 1203, 1140 and 1097 cm^{-1} are assigned to C-O-C bond stretching. In addition, the peaks at 921, 770 and 689 cm^{-1} are related to C-S bond stretching vibrations in the thiophene ring. The presence of PEDOT in V_2O_5/PEDOT is confirmed. From the full XPS survey (Fig. S7 in Supporting information), all the V_2O_5-PEDOT contain V, C and S elements. From the V 2p spectra (Fig. 2b), with the increased of PEDOT content, the V 2p peak shifts towards the lower binding energy, indicating the increase ratio of lower valence state V^{4+} [27]. V 2p peak can be fitted into two peaks V^{5+} and V^{4+}, where the percentage of peak area represents the concentration of each oxidation state of vanadium. With the increase of PEDOT content, V^{5+} decreased to 81.8%, 75.1% and 72.1% for V_2O_5–0.5PEDOT, V_2O_5–1.0PEDOT and V_2O_5–1.5PEDOT, respectively, which should be caused by the oxidative polymerization of EDOT. From the high-resolution C 1s spectra (Fig. 2c), the peaks at 284.8, 286.3, and 288.9 eV are contributed by C-C, C-S, and C-O bonds of the PEDOT, respectively [21]. Fig. 2d depicts the spin-split doublet S 2p peaks of V_2O_5-PEDOT at 163.9 eV (S $2p_{3/2}$) and 165.1 eV (S $2p_{1/2}$), which originate from the thiophene ring of PEDOT [36], while the bands at 168.9 and 169.8 eV come from the S-O bond [37]. With the increase of EDOT content, the peaks of C 1s and S 2p were gradually enhanced.

To evaluate the electrochromic performance reasonably, the film thicknesses were controlled at ~230 nm (Fig. S8 in Supporting information). Transmittance spectra were collected with a voltage ranging from −1.1 V to +0.4 V and wavelength of 350–1000 nm (Figs. 3a-c and S9a in Supporting information). At 422 nm, the ΔT of V_2O_5, V_2O_5–0.5PEDOT, V_2O_5–1.0PEDOT, V_2O_5–1.5PEDOT are 54%, 41.8%, 45%, 41%, respectively. while those at 1000 nm are 39%, 32.8%, 35.2%, 39.8%, respectively. The V_2O_5 with or without the addition of EDOT have quite similar ΔT and relatively high optical contrast, which may be due to the nanostructure morphology. Generally, a strong optical absorption of ~97% for all samples appears in 300–500 nm at 0.4 V, while in the other wavelength range, there is a strong optical transmittance. When the applied voltage decreased to −1.1 V, there is no obvious optical absorption in the spectra. Figs. 3d-f and Fig. S9d (Supporting information) are photographs of color change at different voltages. When the voltage range is from +0.4 V to −1.1 V (*vs.* Ag/Ag^+), the color changes from yellow-green, green, blue-gray and eventually gray. Which is correspondence to the transmittance spectra results. Vanadium ions in V_2O_5-PEDOT films occurred redox reactions between −1.1 V to +0.4 V, resulting in mixing of V^{5+}, V^{4+} and V^{3+} ions in different proportions [38,39]. Different content of V^{5+}, V^{4+} and V^{3+} ions will cause the films to show multi-color changes. The films show rich color variations that are valuable for the study of the esthetic development of electrochromic.

Response time is the time needed to achieve 90% of the maximum transmittance modulation at a specific wavelength [17]. The response time of all samples was tested when the voltage of + 0.4 V and −0.6 V were applied to the film for a pulse time of 30 s respectively (Figs. 4a-c and Fig. S9b in Supporting information). The response times of V_2O_5 and V_2O_5-PEDOT films were summarized in Table S1 (Supporting information). V_2O_5-PEDOT has a faster response time than pure V_2O_5, and V_2O_5–1.0PEDOT has the fastest response time (1.1 s for coloration and 3.5 s for bleaching). It is well known that the electrochromic involves the double implantation of ions and electrons. The ultra-thin nanobelt structure and intercalation of V_2O_5-PEDOT shorten the ion diffusion distance and expands the interlayer spacing, which accelerates the ion diffusion dynamics [25,29]. In addition, PEDOT polymerized in the interlayer can act as a superior electron transport carrier to enhance charge transfer. All these characteristics result in a fast response time for V_2O_5-PEDOT samples. Obviously, the charge transfer resistance decreased with the intercalation of PEDOT. However, the excess PEDOT destroys the crystal structure of V_2O_5. Thus charge transfer resistance of V_2O_5–1.5PEDOT is larger than that of V_2O_5–1.0PEDOT, which accounts for the reduced response time for V_2O_5–1.5PEDOT compared to V_2O_5–1.0PEDOT. Additionally, the coloring time is much shorter than the bleaching time, presumably because the conductivity of vanadium oxide is higher than that of lithium-inserted vanadium oxide [40]. To further investigate the electrochromic performance of V_2O_5-PEDOT (Figs. 4d-f and Fig. S9c in Supporting information), the retentions of original optical contrast for V_2O_5, V_2O_5–0.5 PEDOT, V_2O_5–1.0PEDOT and V_2O_5–1.5PEDOT films are 89%, 95%, 93% and 71% after 1200 cycles. Particularly, the retentions for V_2O_5–0.5PEDOT and V_2O_5–1.0PEDOT are still above 85% after 3000 cycles. Particularly, the retentions for V_2O_5–0.5PEDOT and V_2O_5–1.0PEDOT are still above 85% after 3000 cycles, respectively. It is worth noting that V_2O_5–1.0PEDOT still has a fast response rate ($t_b = 3.8$ s, $t_c = 1.4$ s) after 3000 cycles (Figs. 4g-i). The results show that V_2O_5–1.0PEDOT has good cyclic stability, which is due to the appropriately expand interlayer spacing to mitigate volume expansion.

The formula for coloring efficiency (CE) can be calculated as follows:

$$CE = \Delta OD/Q \quad (1)$$

$$\Delta OD = \log(T_b/T_c) \quad (2)$$

where OD is the change of optical density, Q is the charge per unit area, T_b and T_c refer to the optical transmittance in bleach-

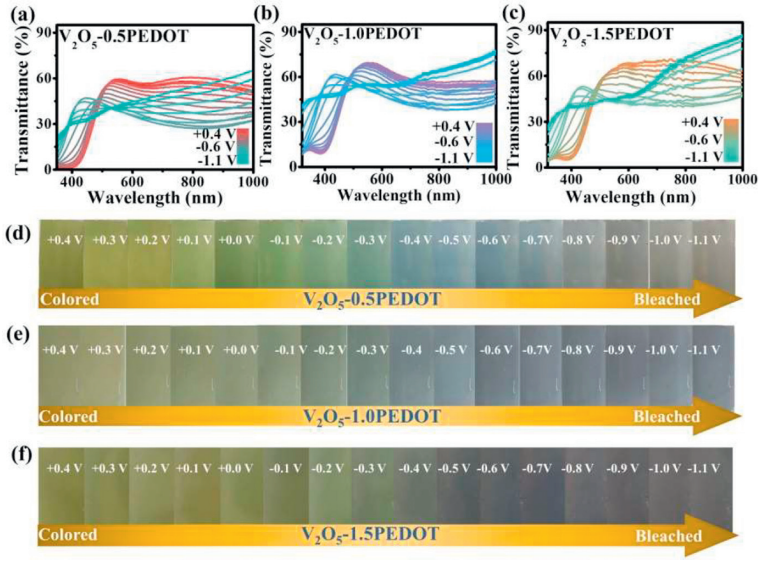

Fig. 3. Spectroelectrochemistry and photographs under different voltages of (a, d) V_2O_5–0.5PEDOT (b, e) V_2O_5–1.0PEDOT (c, f) V_2O_5–1.5PEDOT.

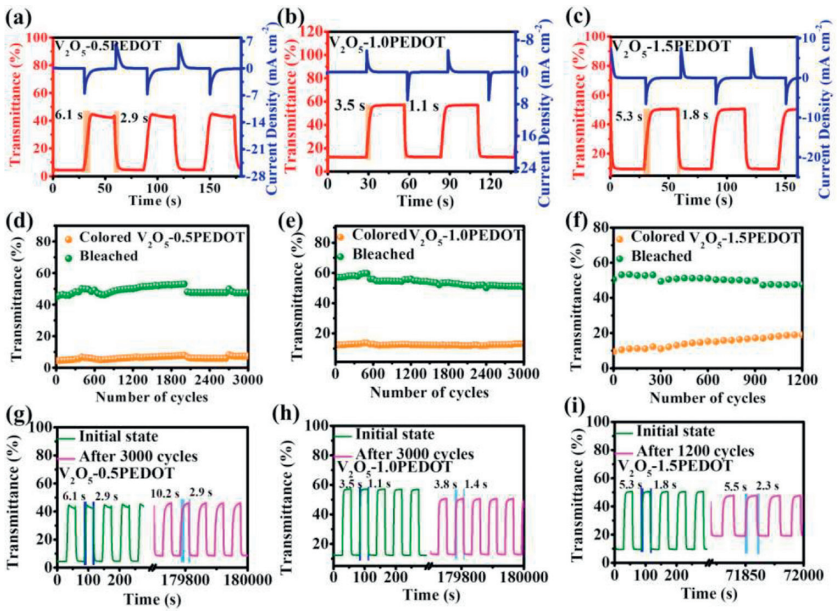

Fig. 4. Response time curves and the stability test of (a, d) V_2O_5–0.5PEDOT (b, e) V_2O_5–1.0PEDOT (c, f) V_2O_5–1.5PEDOT by a voltage between +0.4 V and −0.6 V. Optical contrast curves of (g) V_2O_5–0.5PEDOT (h) V_2O_5–1.0PEDOT (i) V_2O_5–1.5PEDOT films.

ing and coloring states, respectively. Fig. 5a depicts the curves of optical density change with charge density at the optimum wavelength. The *CE* of V_2O_5 nanobelts, V_2O_5–0.5PEDOT, V_2O_5–1.0PEDOT and V_2O_5–1.5PEDOT are 66.3, 76.6, 97.1 and 100.8 cm^2/C, respectively, which is significantly higher than that of other V_2O_5-based electrochromic materials as summarized in Table S1. The coloring efficiency of V_2O_5-PEDOT is much higher than that of V_2O_5. The results indicate that V_2O_5-PEDOT materials only require a relatively small quantity of charge insertion/extraction to obtain significant optical modulation, which is meaningful for energy conservation. In order to investigate the effect of PEDOT on the electrochemical properties of V_2O_5, we performed CV tests on V_2O_5 and V_2O_5-PEDOT films in 1 mol/L $LiClO_4$/PC at a scan rate of 20 mV/s between −1.1 V and +0.4 V (Fig. 5b). There are three pairs of redox peaks A/A', B/B' and C/C', which are caused by Li^+ insertion/extraction accompanied with the reversible transition of valence states between V^{5+}, V^{4+} and V^{3+}. Different voltages could lead to different amount mixture of V^{5+}, V^{4+}, and V^{3+} ions, resulting in more than three color changes in the voltage window as shown in Figs. 3d-f [41]. However, the unmodified V_2O_5 nanobelts present three pairs of broad peaks indicating poor Li^+ insertion/extraction ability. Besides, the area of the CV curve for V_2O_5-PEDOT are larger than that of V_2O_5, indicating better electrochemical activity and faster diffusion kinetics [42]. To analyze the charge transfer kinetics of V_2O_5-PEDOT, the electrochemical impedance spectra (EIS) are performed as shown in Fig. 5c with the inset displaying the fitting circuit model. The R_a is the total resistance of the electrochemical system. The R_{ct} is charge transfer resistance corresponding to the semicircle. The Warburg impedance (Z_W) is a straight line at the low-frequency side, which is related to the ion diffusion on the electrolyte/electrode interface [43]. The R_{ct} of the four samples is shown in Table S2 (Supporting information). V_2O_5–1.0PEDOT has the lowest charge transfer resistance of 41 Ω. Additionally, the slopes of V_2O_5-PEDOT related to Warburg impedance are signifi-

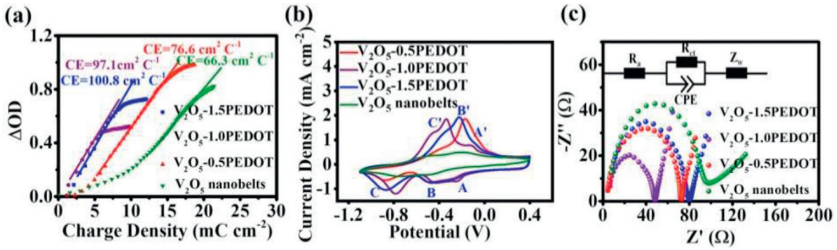

Fig. 5. (a) Variation of the optical density induced per unit of inserted charge for V_2O_5–1.5PEDOT, V_2O_5–1.0PEDOT, V_2O_5–0.5PEDOT films and V_2O_5 nanobelts. (b) Cyclic voltammetry curve. (c) Nyquist plots.

cantly larger than that of V_2O_5 nanobelts, indicating an enhanced ion transfer at the interface. The excellent electronic conductivity of PEDOT and the expanded interlayer spacing are responsible for improved charge and mass transfer at the electrolyte/electrode interface. However, for V_2O_5–1.5PEDOT, the R_{ct} value increased, which may be that excess PEDOT destroys the crystal structure of V_2O_5. The results of Fig. 4 were further verified.

The CV tests at various scanning rates are measured to calculate the diffusion coefficient. As shown in Fig. S10 (Supporting information), the reduction peak moves towards low potential as the scanning rate increases, whereas the oxidation peak moves towards high potential. Thus, redox reactions can utilize the fully active surface area at low scan rates. However, diffusion under high scanning rates restricts Li^+ movement due to time constraint, which enables only exterior active surface to participate in redox reaction and resulting in severe electrode polarization. It can be seen that V_2O_5–1.0PEDOT shows the smallest polarization, which is consistent with EIS results in Fig. 5c. Effective diffusion coefficient can be estimated by the Randles-Servcik equation:

$$i_p = 2.686 \times 10^5 n^{3/2} A D^{1/2} C V^{1/2} \quad (5)$$

where i_p represents the peak current, n is charge transfer number per unit reaction, A is the electrode area, D is the effective diffusion coefficient, C is concentration of Li^+ and v is the potential scan rate. In Fig. S10e-h (Supporting information), the peak current i_p and the square root of the scan rate $v^{1/2}$ show a good linear relationship. The diffusion coefficients are compared with the reported V_2O_5-based nanomaterials summarized in Table S3 (Supporting information). V_2O_5-PEDOT shows superior diffusion coefficients, where V_2O_5–1.0PEDOT exhibits the highest diffusion coefficients of 2.15×10^{-9} cm^2/s (reduction reaction), 8.56×10^{-9} cm^2/s (oxidation reaction), which are 9 times higher than that of V_2O_5 nanobelts.

Finally, the electrochromic device is assembled by using V_2O_5-PEDOT as the electrochromic layer and lithium embedded V_2O_5-PEDOT as ion storage layer as illustrated in Fig. 6a. The color of device changes from yellow-green to green with the voltage ranging from +0 V to −1.4 V, and ΔT is 28.7% in the near infrared region (λ= 1000 nm) as shown in Fig. 6b. Fig. 6c depicts the transmission-time curve with a fast response time (t_b/t_c = 6.66 s/1.28 s) at switching potentials between +0 V and −1.4 V. Herein, the cycling stability is evaluated by capacity retention [44], where the capacity retention is calculated by the ratio of the capacity of the 500th cycle to the capacity of the 2nd cycle. Though the CV curves are somewhat altered, caused by the change of the crystal structure due to Li^+ insertion/extraction [45], the capacity retention is still calculated to be 80% after 500 cycles (Fig. 6d).

In summary, V_2O_5-PEDOT nanobelts with various layer spacings were successfully synthesized by *in situ* intercalation polymerization, and the effect of EDOT on the electrochemical and optical properties was investigated. The intercalation polymerization of PEDOT can expand the interlayer spacing of V_2O_5, thereby accelerating ion insertion/extraction and acting as a conductive pil-

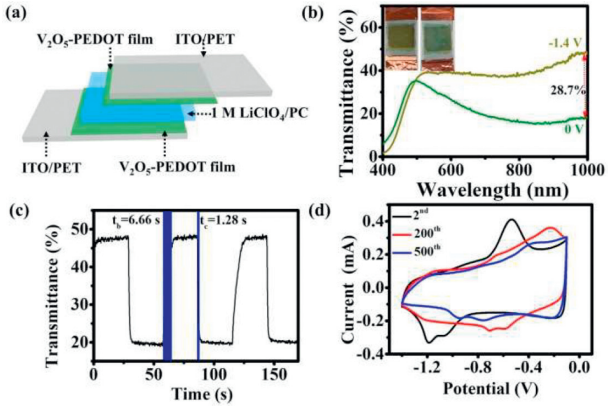

Fig. 6. (a) Schematic of the electrochromic device based on V_2O_5-PEDOT film as the electrochromic layer and ion storage layer. (b) Transmittance spectra and digital photo of ECD. (c) Electrochromic response of ECD at 1000 nm by continuously stepping voltage between +0 V and −1.4 V. (d) CV curves of ECD in 2nd, 200th, 500th cycles.

lar to enhance charge transfer, but excess PEDOT can destroys the crystal structure of V_2O_5. V_2O_5–1.0PEDOT shows the fastest response times (t_c/t_b = 1.1 s/3.5 s) and diffusion rates (8.56×10^{-9} cm^2/s and 2.15×10^{-9} cm^2/s). The ΔT was measured after 3000 cycles and still maintained 86% of the optical contrast and the best response time (t_c/t_b = 1.4 s/3.8 s). Therefore, this work suggests that nanocomposites have better electrochromic properties and have shown significant value in the exploratory studies of ECD.

Declaration of competing interest

The authors declare that they have no known competing financial interests or personal relationships that could have appeared to influence the work reported in this paper.

Acknowledgments

This work was supported by the National Natural Science Foundation of China (No. 51972258), Hubei Natural Science Foundation (No. 2020CFB774), Open Fund by Sanya Science and Education Innovation Park of Wuhan University of Technology (No. 2021KF0021) and the Fundamental Research Funds for the Central Universities (No. WUT:20221VA002). Thanks are given for the measurements supporting from centre for Materials Research and Analysis at Wuhan University of Technology (WUT).

Supplementary materials

Supplementary material associated with this article can be found, in the online version, at doi:10.1016/j.cclet.2023.109213.

References

[1] Z. Wang, W. Gong, X. Wang, et al., ACS Appl. Mater. Interfaces 12 (2020) 33917–33925.
[2] E.L. Runnerstrom, A. Llordes, S.D. Lounis, et al., Chem. Commun. 50 (2014) 10555–10572.
[3] V.K. Thakur, G. Ding, J. Ma, et al., Adv. Mater. 24 (2012) 4071–4096.
[4] P.M. Beaujuge, J.R. Reynolds, Chem. Rev. 110 (2010) 268–320.
[5] A. Balan, D. Baran, L. Toppare, Polym. Chem. 2 (2011) 1029–1043.
[6] C.M. Amb, A.L. Dyer, J.R. Reynolds, Chem. Mater. 23 (2011) 397–415.
[7] H. Park, D.S. Kim, S.Y. Hong, et al., Nanoscale 9 (2017) 7631–7640.
[8] M. Panagopoulou, D. Vernardou, E. Koudoumas, et al., Electrochim. Acta 232 (2017) 54–63.
[9] I. Mjejri, L.M. Manceriu, M. Gaudon, et al., Solid State Ionics 292 (2016) 8–14.
[10] B. Yan, X.F. Li, Z.M. Bai, et al., Nano Energy 24 (2016) 32–44.
[11] H.C. Ho, Y.C. Lai, K. Chen, et al., Appl. Surf. Sci. 495 (2019) 143436.
[12] P. Wei, X. Sun, Z. He, et al., Fuel 339 (2023) 127303.
[13] A.P. Jin, W. Chen, Q.Y. Zhu, et al., Electrochim. Acta 55 (2010) 6408–6414.
[14] W. Yu, J. Wang, Z. Gou, et al., Ceram. Int. 39 (2013) 2639–2643.
[15] H. Zhao, J. Zhong, Y. Qi, et al., Chem. Eng. J. 465 (2023) 143032.
[16] K. Liang, H. Zhao, J. Li, et al., Appl. Surf. Sci. 615 (2023) 156412.
[17] K. Zhang, N. Li, X.X. Ma, et al., J. Electroanal. Chem. 825 (2018) 16–21.
[18] W.J. Li, C. Han, Q.F. Gu, et al., Adv. Energy Mater. 10 (2020) 2001852.
[19] A.V. Murugan, B.B. Kale, C.W. Kwon, et al., J. Mater. Chem. 11 (2001) 2470–2475.
[20] B.L. Groenendaal, F. Jonas, D. Freitag, et al., Adv. Mater. 12 (2000) 481–494.
[21] D.M. Xu, H.W. Wang, F.Y. Li, et al., Adv. Mater. Interfaces 6 (2019) 1801506.
[22] C.X. Guo, G. Yilmaz, S.C. Chen, et al., Nano Energy 12 (2015) 76–87.
[23] H. Ling, L. Liu, P.S. Lee, et al., Electrochim. Acta 174 (2015) 57–65.
[24] H. Ling, G. Ding, D. Mandler, et al., Chem. Commun. 52 (2016) 9379–9382.
[25] S.F. Kuchena, Y. Wang, Electrochim. Acta 425 (2022) 140751.
[26] S.H. Zhang, Y.H. Zhao, Z.F. Du, et al., Sol. Energy Mater. Sol. Cells 207 (2020) 110354.
[27] P. Yang, P. Sun, W. Mai, Mater. Today 19 (2016) 394–402.
[28] W. Bi, E. Jahrman, G. Seidler, et al., ACS Appl. Mater. Interfaces 11 (2019) 16647–16655.
[29] C.X. Guo, K. Sun, J.Y. Ouyang, et al., Chem. Mater. 27 (2015) 5813–5819.
[30] X. Rui, Y. Tang, O.I. Malyi, et al., Nano Energy 22 (2016) 583–593.
[31] K. Liang, H. Zhao, J. Li, et al., Small 19 (2023) 2207562.
[32] S.L. Li, X.J. Wei, C.H. Wu, et al., ACS Appl. Energy Mater. 4 (2021) 4208–4216.
[33] V. Petkov, P.N. Trikalitis, E.S. Bozin, et al., J. Am. Chem. Soc. 124 (2002) 10157–10162.
[34] Z.G. Yao, Q.P. Wu, K.Y. Chen, et al., Energy Environ. Sci. 13 (2020) 3149–3163.
[35] D. Bin, W.C. Huo, Y.B. Yuan, et al., Chem 6 (2020) 968–984.
[36] Z. Liu, J. Xu, R. Yue, et al., Electrochim. Acta 196 (2016) 1–12.
[37] D. Wu, W. Zhang, Y. Feng, et al., J. Mater. Chem. A 8 (2020) 2618–2626.
[38] Z.Q. Tong, N. Li, H.M. Lv, et al., Sol. Energy Mater. Sol. Cells 146 (2016) 135–143.
[39] Y.S. Hsiao, C.W. Chang-Jian, W.L. Syu, et al., Appl. Surf. Sci. 542 (2021) 148498.
[40] D.R. Rolison, B. Dunn, J. Mater. Chem. 11 (2001) 963–980.
[41] Z. Tong, X. Zhang, H. Lv, et al., Adv. Mater. Interfaces 2 (2015) 1570085.
[42] Y. Lu, L. Liu, D. Mandler, et al., J. Mater. Chem. C 1 (2013) 7380–7386.
[43] H.Y. Liu, X.P. Liang, T. Jiang, et al., Electrochim. Acta 404 (2022) 139784.
[44] I. Mjejri, M. Gaudon, A. Rougier, Sol. Energy Mater. Sol. Cells 198 (2019) 19–25.
[45] M. Panagopoulou, D. Vernardou, E. Koudoumas, et al., Electrochim. Acta 321 (2019) 134743.